ACCEPTED MANUSCRIPT
Review of Scientific Instruments
AIP Publishing
This is the author's peer reviewed, accepted manuscript. However, the online version of record will be different from this version once it has been copyedited and typeset.
PLEASE CITE THIS ARTICLE AS DOI: 10.1063/5.0205656

3D reconstruction of an inertial-confinement fusion implosion with neural networks using multiple heterogeneous data sources

J. H. Kunimune,[1, a)] D. T. Casey,[2] B. Kustowski,[2] V. Geppert-Kleinrath,[3] L. Divol,[2] D. N. Fittinghoff,[2] P. L. Volegov,[3] M. K. G. Kruse,[2] J. A. Gaffney,[2] R. C. Nora,[2] and J. A. Frenje[1]
[1)] *Plasma Science and Fusion Center, Massachusetts Institute of Technology. 167 Albany St., Cambridge, MA, USA. 02139.*
[2)] *Lawrence Livermore National Laboratory. 7000 East Ave., Livermore, CA, USA. 94550.*
[3)] *Los Alamos National Laboratory. P.O. Box 1663, Los Alamos, NM, USA. 87545.*

(Dated: 19 June 2024)

3D asymmetries are major degradation mechanisms in inertial-confinement fusion implosions at the National Ignition Facility (NIF). These asymmetries can be diagnosed and reconstructed with the neutron imaging system (NIS) on three lines of sight around the NIF target chamber. Conventional tomographic reconstructions are used to reconstruct the 3D morphology of the implosion using NIS [P. L. Volegov et al., J. Appl. Phys. **127**, 083301 (2020)], but the problem is ill-posed with only three imaging lines of sight. Asymmetries can also be diagnosed with the real-time neutron activation diagnostics (RTNAD) and the neutron time-of-flight (nToF) suite. Since NIS, RTNAD, and nToF each sample a different part of the implosion using different physical principles, we propose it is possible to overcome the limitations of too few imaging lines of sight by performing 3D reconstructions that combine information from all three heterogeneous data sources. This work presents a new machine learning-based reconstruction technique to do just this. By using a simple physics model and group of neural networks to map 3D morphologies to data, this technique can easily account for data of multiple different types. A simple proof-of-principle is presented, demonstrating that this technique can accurately reconstruct a hot-spot shape using synthetic primary neutron images and a hot-spot velocity vector. In particular, the hot-spot's asymmetry, quantified as spherical harmonic coefficients, is reconstructed to within ±4% of the radius in 90% of test cases. In the future, this technique will be applied to actual NIS, RTNAD, and nToF data to better understand 3D asymmetries at the NIF.

I. INTRODUCTION

The goal of an inertial-confinement fusion (ICF) experiment at the National Ignition Facility (NIF)[1] is to compress a spherical capsule of deuterium-tritium (DT) fuel to high enough temperatures and pressures to achieve fusion ignition and produce high energy gain ($G \gg 1$). While a few NIF experiments have achieved ignition[2] and energy gain,[3] there are still many degradation mechanisms that terminate the burn early and prevent the experiments from reaching their maximum possible gain. One of the dominant degradation mechanisms is 3D asymmetries,[4,5] which are seeded by asymmetry in the laser drive and engineering features in the hohlraum and capsule. They prevent efficient compression of the capsule and result in large flows at minimum-volume. Those flows contain residual kinetic energy – which would otherwise contribute internal energy to the burning hot-spot – and enhance the $p\,\mathrm{d}V$ losses that eventually terminate the burn wave.[6]

To better optimize implosion designs for higher gains, it is necessary to understand these low-mode asymmetries in 3D. To this end, many diagnostics have been installed around the NIF target chamber to build an understanding of the implosion morphology in 3D.[7] One is the neutron imaging system (NIS), which collects primary neutron images from three lines of sight and down-scattered neutron images from two lines of sight.[8] Another is the suite of neutron time-of-flight (nToF) detectors, which collect neutron spectra along seven lines of sight, from which the 3D velocity vector of the burning hot-spot is inferred.[9] Another is the array of real-time neutron activation diagnostics (RTNADs), which collects primary neutron yield on 48 different lines of sight, from which the areal density along those 48 lines of sight is inferred.[10]

These diagnostics sample different parts of the implosion using different physical principles, and provide different types of information. This results in heterogeneous data that is difficult to compare and combine. There currently exist techniques to infer the 3D morphology of the implosion using just NIS images[11] or just RTNAD data.[10] However, as only three NIS lines of sight exist, reconstructing a 3D morphology is an ill-posed problem often requiring assumptions about symmetry (e.g. cylindrical symmetry) to solve,[12] and the RTNADs are limited in that they are insensitive to radial profiles and higher-mode asymmetries. In general, increasing the number of measurements and the number of lines of sight increases the accuracy with which the 3D source can be reconstructed.[12] Thus, ideally, any reconstruction of the implosion morphology should simultaneously account for all of the 3D data available, including NIS, nToF, and RTNAD data. However, the analytic methods used to

[a)] Author to whom correspondence should be addressed: kunimune@mit.edu

ACCEPTED MANUSCRIPT
Review of Scientific Instruments
AIP Publishing
This is the author's peer reviewed, accepted manuscript. However, the online version of record will be different from this version once it has been copyedited and typeset.
PLEASE CITE THIS ARTICLE AS DOI: 10.1063/5.0205656

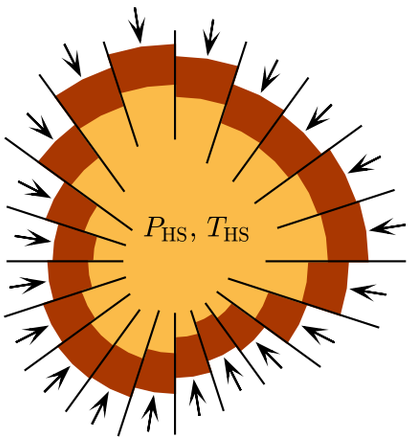

FIG. 1. An ICF implosion as represented by the rocket-piston model.[20] The red pistons of shell material[21] are accelerated inward by the ablation pressure[22,23] and by outward by the hot-spot pressure.[24]

perform existing reconstructions, such as computed tomographic algorithms,[11,13,14] cannot easily account for multiple different types of data at once (e.g. primary neutrons, down-scattered neutrons, and x-rays; or scalars, vectors, and images).

A technique commonly used to solve inverse problems like this one is forward-fitting.[15,16] The implosion morphology is parameterized by some model, and a method is developed to generate synthetic data given a morphology. The synthetic data can subsequently be treated as a function of the morphology parameters. Given real data, the function is inverted by an iterative optimization algorithm like gradient descent or Levenberg–Marquardt[17] to find the parameters that generate the synthetic data that most closely matches the real data. Because forward-fitting is general, it can easily account for data of multiple different types simultaneously. However, since it relies on an iterative optimization algorithm, it can also be quite slow. In complex problems, forward-fitting also tends to suffer from getting stuck in local minima.

One approach that has gained popularity in recent years for its ability to speed up previously slow calculations is artificial neural networks.[14,18,19] In this paper, we present a technique that uses neural networks with a physics model to reconstruct the 3D morphology of an ICF implosion using NIS and nToF data in a manner similar to but faster and more robust than a forward-fit.

II. 3D ROCKET-PISTON MODEL

The first component of this technique is a model to parameterize the implosion morphology and generate synthetic data. A 3D multiple rocket-piston model is used as described by Casey et al.[20] and illustrated in Figure 1. This model extends Hurricane et al.'s implosion asymmetry model.[21] The shell is represented as an arbitrary number of massive pistons, which impinge on an isobaric hot-spot. It solves the equations of motion of the pistons coupled with Callahan et al.'s hohlraum radiation model,[22] Olson et al.'s x-ray ablation model,[23] and Springer et al.'s hot-spot power-balance model[24] to provide a holistic but simplified model of an ICF experiment.

A physics model is used rather than a purely geometric model like spherical harmonic[15] or voxel[11] decomposition, because it forces the reconstructions to be physically possible, which helps with the ill-posed nature of the problem. It also naturally couples purely geometric quantities like hot-spot radius to non-geometric quantities like hot-spot velocity. The disadvantage of a physics model is that it fails to reconstruct data that contains physics not included in the model. However, this model sufficiently captures the physics expected to be probed with NIS, nToF, and RTNADs. The reason this model is used rather than a higher-fidelity physics model like HYDRA[25] is because the increased speed of the rocket-piston model allows the generation of synthetic data more quickly. However, the workflow and techniques developed here can be extended or refined with models like HYDRA in the future.

To generate synthetic NIS data, a 2D projection of the 3D neutron emission profile is performed along each of the three NIS lines of sight. This provides a good approximation of primary neutron images without any noise or background, but cannot produce down-scattered neutron images. Means of calculating down-scattered neutron images will be implemented in the future. Each image is translated so that its center-of-mass is on the origin, since real NIS images do not contain absolute positioning information. The 3D hot-spot velocity vector is calculated as the average velocity of the multiple pistons. Other measurable quantities, specifically the total yield, the ion temperature, and the burn-duration, are extracted from the power-balance model.

To produce enough data to enable machine learning, this rocket-piston model is executed 62 000 times. This was the number of executions that could complete in 192 CPU-hours. This was chosen because the model trained on 31 000 samples showed signs of overfitting (outputs based on training samples were noticeably more accurate than outputs based on samples not used in the training), while the model trained on 62 000 samples did not. Even more samples would yield better results, at the cost of even more computation time.

The goal is to create a dataset that captures all of the key modes of variation in the model. Accordingly, each of the runs is a random perturbation of a point design: a 2.271 mm outer-diameter capsule with a 85 µm thick diamond ablator and a 65 µm thick cryogenic DT ice layer. The time-resolved drive pressure is tuned to match DANTE measurements from the NIF shot on 2022

ACCEPTED MANUSCRIPT
Review of Scientific Instruments
AIP Publishing
This is the author's peer reviewed, accepted manuscript. However, the online version of record will be different from this version once it has been copyedited and typeset.
PLEASE CITE THIS ARTICLE AS DOI: 10.1063/5.0205656

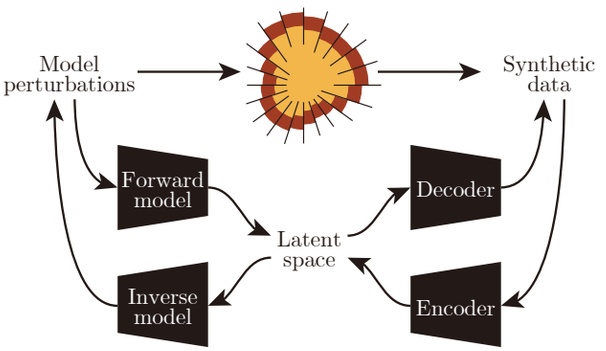

FIG. 2. A schematic representation of the manifold- and cyclically-consistent[26] collection of neural networks applied in this work. The *model perturbations* are the ten perturbations to the point-design that are input to the rocket-piston model, the *synthetic data* is the NIS images and nToF scalars output by the rocket-piston model, and the *latent space* is a compressed representation of the synthetic data. The rocket-piston model, represented by the red and yellow implosion, maps a set of model perturbations to synthetic data, while the neural networks, represented by the black boxes, map model perturbations and synthetic data into and out of the latent space.

September 19.[3] Zero-dimensional variation is seeded by applying normally-distributed perturbations to the drive strength, shell mass, and initial fill temperature. Asymmetry is seeded by applying shell-mass perturbations with certain spherical harmonic modes Y_l^m, with magnitudes drawn from a normal distribution. Specifically, the varied modes are $Y_{l=1}^{m=0}$, $Y_{l=1}^{m=\pm1}$, $Y_{l=2}^{m=0}$, $Y_{l=2}^{m=\pm2}$, and $Y_{l=4}^{m=0}$. For this proof of principle study, restricting variation to these seven modes and three scalars simplifies the training by reducing the dimensionality of the solution space.

The power balance equations are simplified for the same reason, using the constraint that $pV^\gamma = \text{constant}$, which assumes that alpha heating and radiation losses are approximately equal. This is valid for low-to-moderate levels of alpha heating. This simplifies the training by improving the smoothness of the solution space.

The shape perturbations are all on the order of a few percent. However, they grow during the implosion process such that by the time of minimum volume, the asymmetries are on the order of 20% the hot-spot radius, and hot-spot velocity is on the order of $50\,\mathrm{km\,s^{-1}}$.

III. SURROGATE MODEL

To facilitate fast execution and inversion, the dataset generated with the rocket-piston model is used to train a surrogate model. The surrogate model is a collection of four neural networks arranged according to the principle of manifold- and cyclical-consistency, as described by Anirudh et al.[26] and illustrated in Figure 2. An encoder network and a decoder network (each with three hidden convolutional layers and two hidden fully-connected layers) map the data from each implosion to a point in a 32-dimensional latent space (a compressed representation of the data), a forward model network (with three hidden fully-connected layers) maps a set of model perturbations to the corresponding point in the latent space in accordance with the rocket-piston model, and an inverse model network (with three hidden fully-connected layers) maps each point in the latent space to a set of model perturbations. All four networks use the rectified linear unit as their activation function, and are structured to allow images as inputs or outputs along with scalars. Specifically, inputs and outputs in the data space comprise the three primary NIS images, the x, y, and z components of the hot-spot velocity, the bang-time, the burn-averaged ion temperature, and the logarithm of the total yield.

The networks are trained in two stages – first the encoder and decoder networks are trained on the synthetic data to allow a set of data to be fed through the encoder network and then back through the decoder network without losing any information. This takes 40 000 iterations, and defines the latent space such that it represents the principal degrees of freedom in the synthetic data. The forward model and inverse model networks are then trained to mimic the rocket-piston model as closely as possible. This takes 400 000 iterations. More details on the particular implementation of this architecture and the training process are reported by Kustowski et al.[27]

This architecture is motivated by two factors. First, using four interconnected networks in this arrangement, rather than a single network that maps model perturbations to synthetic data, smooths out the prediction space, resulting in better predictions when the amount of data is limited.[26] Second, this surrogate model is fully invertible, making it efficient to not only generate synthetic data corresponding to a set of model perturbations (that is, the function of the rocket-piston model), but also to calculate the model perturbations corresponding to a set of data (that is, a 3D reconstruction of the implosion).

When ground truth and reconstructed images are compared in the process of training the networks, they are normalized to a mean pixel value of one, and subsequently compared on a pixel-by-pixel basis.

IV. PROOF-OF-PRINCIPLE WITH SYNTHETIC DATA

With the rocket-piston model and trained surrogate model, it is now possible to perform 3D reconstructions. Synthetic data is used to test this capability and determine how accurate the resulting reconstructions are.

First, to validate that the surrogate model mimics the rocket-piston model, 1000 samples that were not used for the training process are fed into the neural networks. Model perturbations are fed through the forward model network into the latent space and then through the de-

ACCEPTED MANUSCRIPT
Review of Scientific Instruments
AIP Publishing
This is the author's peer reviewed, accepted manuscript. However, the online version of record will be different from this version once it has been copyedited and typeset.
PLEASE CITE THIS ARTICLE AS DOI: 10.1063/5.0205656

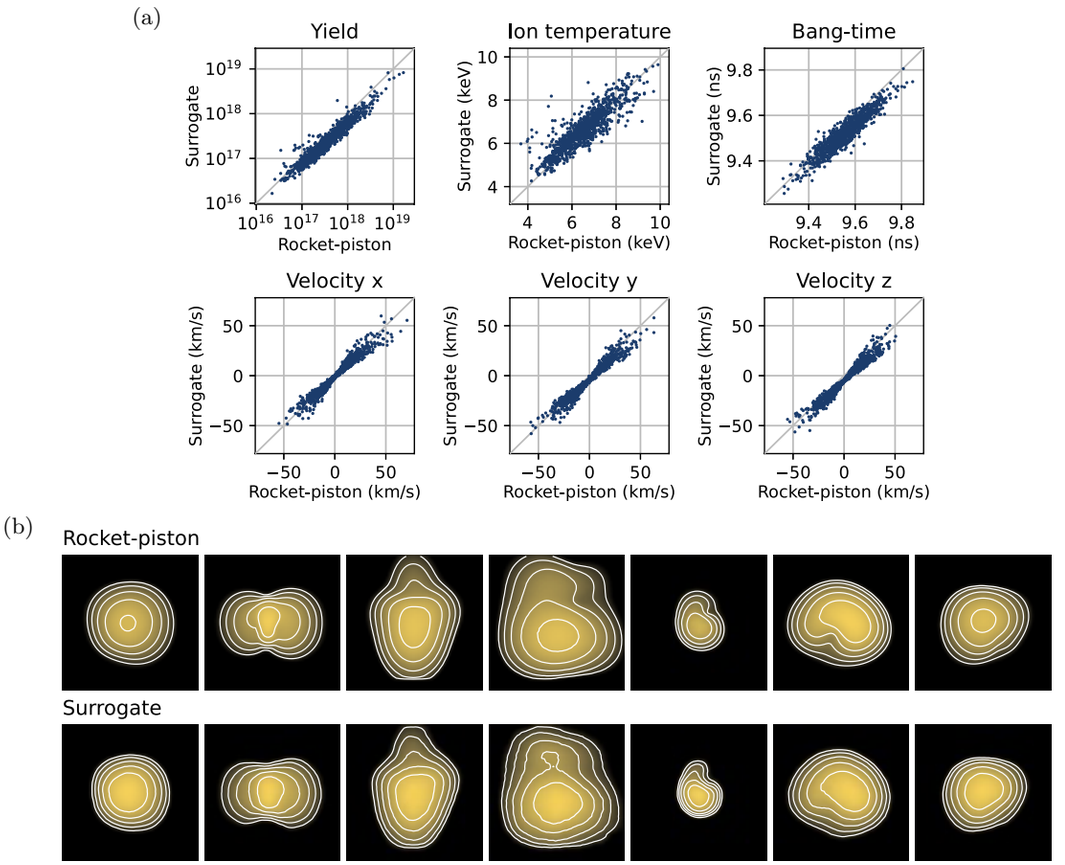

FIG. 3. (a) Each point is synthetic data from one perturbed rocket-piston simulation that was not used in the training process. The x-axis is the value produced by the rocket-piston model, and the y-axis is the value produced by the surrogate model. The points lie near the line $y = x$, indicating that the surrogate model matches the rocket-piston model closely. (b) Each column is the primary neutron image from a particular line of sight for a perturbed rocket-piston simulation. The top image in each column is produced by the rocket-piston model, and the bottom image is produced by the surrogate model. The top and bottom rows look similar, indicating that the surrogate model matches the rocket-piston model closely.

coder network into data space. The result is compared to the synthetic data produced by the rocket-piston model for the same set of perturbations. The comparison for many sets of perturbations is shown in Figure 3. The result from the neural networks matches the result from the rocket-piston model closely, indicating that the surrogate model mimics the rocket-piston model well.

Next, to validate the utility of the networks for 3D reconstruction, synthetic data is generated by the rocket-piston model, then fed through the encoder network into the latent space and through the inverse model network into the perturbation space. This provides a reconstruction of the model perturbations that correspond to the synthetic data, which is compared to the original model perturbations. The comparison for 1000 sets of perturbations is shown in Figure 4. The reconstruction from the neural networks matches the original model perturbations closely, indicating that the surrogate model can be used to infer the model perturbations that were used to generate any given synthetic data.

Finally, to demonstrate how this surrogate model would be used in reality, the reconstructed model perturbations are passed through the rocket-piston model one more time. The hot-spot morphology at bang-time, defined by the positions and velocities of the pistons, is extracted. The comparison of this reconstructed morphology to the original morphology used to generate the data is shown for one test sample in Figure 5, showing a good agreement, demonstrating that the surrogate model was used successfully to infer the hot-spot morphology from NIS and nToF data.

A spherical harmonic decomposition is used to quantify the accuracy with which the reconstruction captures the hot-spot shape. Because the rocket-piston model represents the boundary between the burning hot-spot and the dense fuel as a discontinuous surface (rather than a continuous transition as it is in reality), the boundary can be expressed exactly in spherical coordinates and fit

ACCEPTED MANUSCRIPT
Review of Scientific Instruments
AIP Publishing
This is the author's peer reviewed, accepted manuscript. However, the online version of record will be different from this version once it has been copyedited and typeset.
PLEASE CITE THIS ARTICLE AS DOI: 10.1063/5.0205656

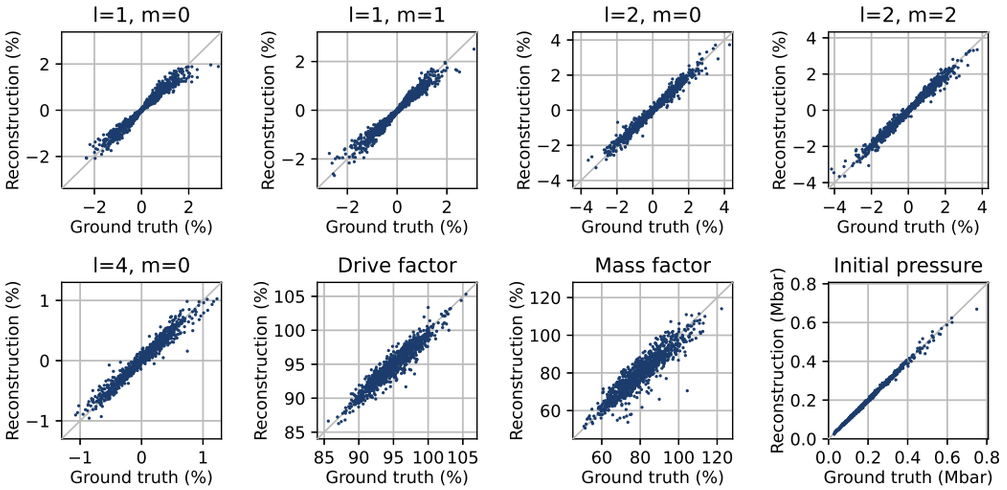

FIG. 4. Each point is a perturbed rocket-piston simulation that was not used in the training process. The x-axis is the original perturbation fed into the rocket-piston model, and the y-axis is the value obtained after passing the resulting synthetic data through the surrogate model. The points lie near the line $y = x$, indicating that the input perturbations can be inferred from the synthetic data using the surrogate model.

to a sum of spherical harmonics:

$$r_{\text{hot-spot}}(\theta,\phi) \approx A_{0,0}\left(1+\sum_{l=1}^{5}\sum_{m=-l}^{l} a_{l,m}\, Y_l^m(\theta,\phi)\right) \quad (1)$$

The spherical harmonic coefficients $a_{l,m}$ quantify deviations from a spherical shape at bang-time, relative to the angularly-averaged hot-spot radius. These shape coefficients, along with the components of the hot-spot velocity vector, are compared for both the original hot-spot morphology and the reconstructed hot-spot morphology. This comparison is repeated for 100 reconstructions and shown in Figure 6. The reconstructed morphologies' shape coefficients match the true morphologies' shape coefficients to within $\pm.065$ for $l = 1$ modes, within $\pm.105$ for $l = 2$ modes, within $\pm.008$ for $l = 3$ modes, within $\pm.060$ for $l = 4$ modes, and within $\pm.005$ for $l = 5$ modes (though since $l = 3$ and $l = 5$ modes were not seeded, the true values of those coefficients never exceed .03), and the reconstructed velocity components match the true velocity components to within $\pm 17.2\,\mathrm{km\,s^{-1}}$. This accuracy is sufficient for knowing the qualitative asymmetry of an implosion. In addition, the reconstruction is usually much closer than these numbers would suggest. In 90% of test cases, shape coefficients match to within $\pm.024$ for $l = 1$, within $\pm.034$ for $l = 2$, and within $\pm.013$ for $l = 4$, and velocity components match to within $\pm 5.9\,\mathrm{km\,s^{-1}}$.

These comparisons show that this methodology can be used for 3D reconstructions of NIF implosions using data with multiple different shapes. Deviations from a perfect match are caused by the limited size of the latent space, the limited size of the neural networks, the finite number of training data, and the finite number of training iterations. Increasing the size of the latent space and networks would improve the quality of the match but increase the risk of overfitting and producing the wrong answer. Increasing the number of training data and training iterations would also increase the quality of the match but also increase the amount of computing resources needed to train the surrogate model.

V. FUTURE WORK

A limitation of this direct-inversion implementation as implemented here is that it does not account for uncertainty in the data. The technique as described here answers the question "what single implosion morphology best corresponds to this data?" rather than the more important question "what set of implosion morphologies might plausibly correspond to this data?" To address this, uncertainty quantification will be implemented. This can be done by propagating uncertainties from the measurements through the neural network, or by using Bayesian analysis with Markov chain Monte Carlo[28] to sample the set of all reconstructions that are consistent with the data. Rigorous uncertainty quantification will make it possible to say how accurate one can expect the reconstruction to be (that is, whether it is one of the 90% of test cases with improved accuracy), without looking at the ground truth. This will also enable rigorous studies of how the number of detectors and detector resolution affect the reconstruction accuracy.

While this technique works well for synthetic data, it must be refined before it can be used to reliably reconstruct real NIF data. In particular, it will be trained on more realistic simulations – including burn physics, more perturbation modes, and background and noise. In

ACCEPTED MANUSCRIPT
Review of Scientific Instruments
AIP Publishing
This is the author's peer reviewed, accepted manuscript. However, the online version of record will be different from this version once it has been copyedited and typeset.
PLEASE CITE THIS ARTICLE AS DOI: 10.1063/5.0205656

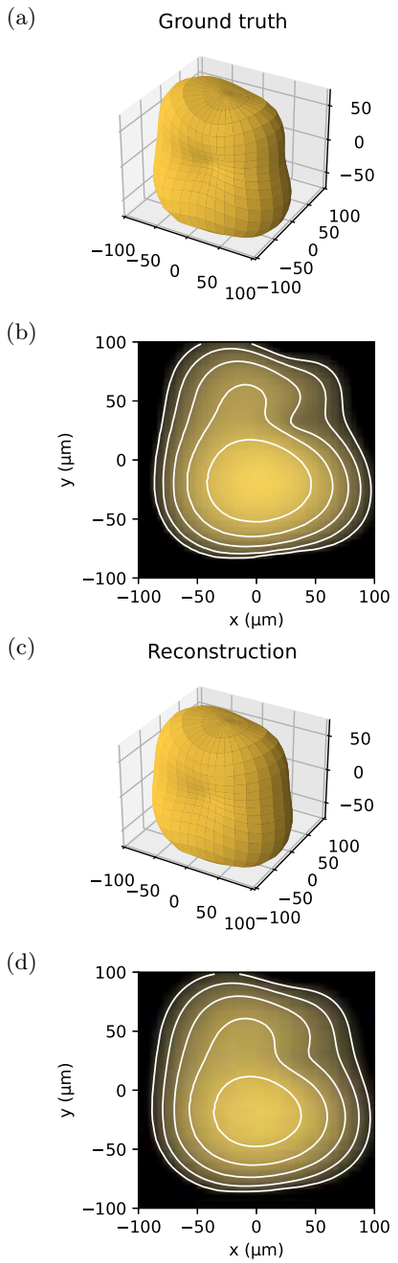

FIG. 5. (a) A 3D hot-spot shape at bang-time extracted from a perturbed rocket-piston simulation that was not used in the training process. Because the rocket-piston model represents the hot-spot boundary as a discontinuous surface, it can be plotted exactly in space. (b) A primary neutron image from that simulation for one line of sight. (c) The 3D hot-spot shape resulting from passing the synthetic data (including all three images, not just the one shown in b.) through the surrogate model and then feeding the resulting perturbations into the rocket-piston model. It looks similar to the shape shown in a., indicating that the 3D hot-spot shape has been reconstructed from the synthetic data. (d) A primary neutron image from the second rocket-piston simulation for the same line of sight. It looks similar to the image in b., indicating that the reconstruction is consistent with the synthetic data it was based on.

addition, asymmetry in the shell density is particularly important to implosion performance, but is not probed by primary neutron images or nToF data. To expand beyond the burning hot-spot asymmetry and infer the shell density as well, the dataset will also be expanded to use down-scattered images and RTNAD data. Incorporating these features will make the surrogate model more difficult to train, mandating a larger dataset and larger neural networks. But ultimately, this will result in reconstructions that use more data and heterogeneous data types than traditional techniques, providing a more accurate and more detailed understanding of the implosion.

Once this technique has been fully implemented for use on neutron data obtained at the NIF, it will be generalized to other ICF applications. While in many cases it will not provide benefits beyond what conventional analysis techniques can do, it has great potential in any situation where multiple diagnostics that probe related physics are used to obtain different types of data (scalars, vectors, images, or time-series) that cannot be combined using traditional techniques. For example, gamma-ray[8] and x-ray[13] diagnostics can be used instead of or in addition to neutron diagnostics. This should require little modification to what is presented here – the step in the model that converts the implosion morphology to synthetic data must be altered such that it generates x-ray data instead of neutron data. Similarly, at the OMEGA laser facility, 3D reconstructions of knock-on deuteron images[29,30] have proven difficult to perform with conventional tomographic or forward-fitting techniques, and will likely benefit from this approach. Again, the only required change would be producing knock-on deuteron images instead of neutron images.

VI. SUMMARY

Ignition and energy gain have been achieved with a few ICF experiments at the NIF, but these implosions still suffer from various degradation mechanisms that terminate the burn and limit gain. The dominant degradation mechanism is 3D low-mode asymmetries. Asymmetries are diagnosed by a variety of instruments positioned around the NIF target chamber. These include the NIS, the RTNADs, and the nToF suite. While all of these diagnostics are routinely used to make inferences about the 3D morphologies of ICF implosions, each is limited in different ways and thus only captures part of the implosion. Ideally, any 3D reconstruction technique should combine all available information from multiple diagnostics. However, conventional analytic techniques cannot easily account for data with multiple different types.

To remedy this issue, a new technique is introduced based on neural networks to perform this reconstruction. A 3D multiple rocket-piston model is used to map input perturbations to synthetic data. This rocket-piston model couples existing models of hohlraum radiation and

ACCEPTED MANUSCRIPT
Review of Scientific Instruments
AIP Publishing
This is the author's peer reviewed, accepted manuscript. However, the online version of record will be different from this version once it has been copyedited and typeset.
PLEASE CITE THIS ARTICLE AS DOI: 10.1063/5.0205656

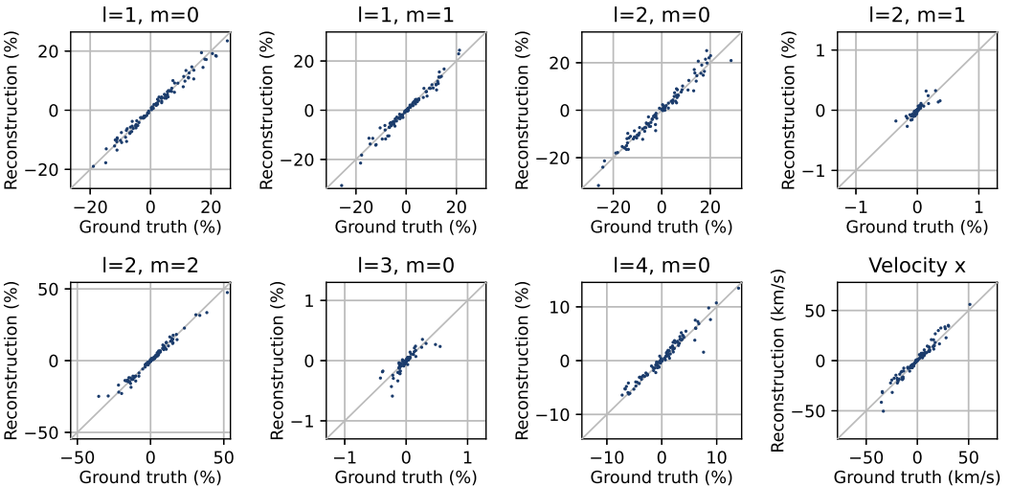

FIG. 6. Each point is a hot-spot morphology from a perturbed rocket-piston simulation that was not used in the training process. The x-axis is a spherical harmonic coefficient or a velocity component for the true morphology, and the y-axis is the same coefficient or component for the morphology reconstructed from the corresponding synthetic data using the surrogate model. The maximum deviation of the points from $y = x$ quantifies the uncertainty of these hot-spot morphology reconstructions.

x-ray ablation to an arbitrary number of massive pistons impinging on an isobaric hot-spot. Synthetic data are generated and used to train a surrogate model, composed of four neural networks, to mimic the rocket-piston model. Inverting this surrogate model allows for the reconstruction of an implosion morphology from a set of data. Because this technique is general, it can easily account for data with multiple different types.

A simple proof-of-principle has been performed, which shows that this methodology can accurately reconstruct a 3D hot-spot morphology using synthetic primary neutron images, the 3D hot-spot velocity vector, and other scalar data. In particular, it reconstructs the magnitude of the hot-spot's asymmetries, quantified as spherical harmonic coefficients, to within $\pm.034$ times the hot-spot radius in 90% of test cases and within $\pm.105$ times the hot-spot radius in the worst test case. It also reconstructs the hot-spot velocity vector to within $\pm 5.9\,\mathrm{km\,s^{-1}}$ in 90% of cases and within $\pm 17.2\,\mathrm{km\,s^{-1}}$ in the worst case. However, there is much work to be done before it is suitable to be applied to real NIF data. Bayesian methods will be implemented to properly account for measurement uncertainty. In addition, the synthetic dataset will be expanded to incorporate down-scattered neutron images and RTNAD data, and refined to better match reality. Once this is done, this technique will provide a valuable and unique tool for better understanding 3D asymmetries at NIF and other ICF facilities.

ACKNOWLEDGMENTS

This work was performed under the auspices of the U.S. Department of Energy by Lawrence Livermore National Laboratory under Contract DE-AC52-07NA27344. This work was also supported in part by the U.S. Department of Energy NNSA MIT Center-of-Excellence under Contract DE-NA0003868, and by the NNSA Laboratory Residency Graduate Fellowship under Contract DE-NA0003960.

This report was prepared as an account of work sponsored by an agency of the United States Government. Neither the United States Government nor any agency thereof, nor any of their employees, makes any warranty, express or implied, or assumes any legal liability or responsibility for the accuracy, completeness, or usefulness of any information, apparatus, product, or process disclosed, or represents that its use would not infringe privately owned rights. Reference herein to any specific commercial product, process, or service by trade name, trademark, manufacturer, or otherwise does not necessarily constitute or imply its endorsement, recommendation, or favoring by the United States Government or any agency thereof. The views and opinions of authors expressed herein do not necessarily state or reflect those of the United States Government or any agency thereof.

This document has been reviewed for release as document LLNL-JRNL-860412.

AUTHOR DECLARATIONS

The authors have no conflicts to disclose.

ACCEPTED MANUSCRIPT
Review of Scientific Instruments
AIP Publishing
This is the author's peer reviewed, accepted manuscript. However, the online version of record will be different from this version once it has been copyedited and typeset.
PLEASE CITE THIS ARTICLE AS DOI: 10.1063/5.0205656

DATA AVAILABILITY STATEMENT

The data that support the findings of this study are available from the corresponding author upon reasonable request.

REFERENCES

[1]G. H. Miller, E. I. Moses, and C. R. Wuest, "The National Ignition Facility: enabling fusion ignition for the 21st century," Nuclear Fusion **44**, S228–S238 (2004).
[2]H. Abu-Shawareb, R. Acree, P. Adams, J. Adams, B. Addis, R. Aden, and P. Adrian (Indirect Drive ICF Collaboration), "Lawson criterion for ignition exceeded in an inertial fusion experiment," Physical Review Letters **129**, 075001 (2022).
[3]H. Abu-Shawareb, R. Acree, P. Adams, J. Adams, B. Addis, R. Aden, and P. Adrian (The Indirect Drive ICF Collaboration), "Achievement of target gain larger than unity in an inertial fusion experiment," Physical Review Letters **132**, 065102 (2024).
[4]D. T. Casey, B. J. MacGowan, J. D. Sater, A. B. Zylstra, O. L. Landen, J. Milovich, O. A. Hurricane, A. L. Kritcher, M. Hohenberger, K. Baker, S. Le Pape, T. Döppner, C. Weber, H. Huang, C. Kong, J. Biener, C. V. Young, S. Haan, R. C. Nora, S. Ross, H. Robey, M. Stadermann, A. Nikroo, D. A. Callahan, R. M. Bionta, K. D. Hahn, A. S. Moore, D. Schlossberg, M. Bruhn, K. Sequoia, N. Rice, M. Farrell, and C. Wild, "Evidence of three-dimensional asymmetries seeded by high-density carbon-ablator nonuniformity in experiments at the national ignition facility," Physical Review Letters **126**, 025002 (2021).
[5]D. Casey, B. MacGowan, O. Hurricane, O. Landen, R. Nora, S. Haan, A. Kritcher, A. Zylstra, J. Ralph, E. Dewald, M. Hohenberger, A. Pak, P. Springer, C. Weber, J. Milovich, L. Divol, E. Hartouni, R. Bionta, K. Hahn, D. Schlossberg, A. Moore, and M. Gatu Johnson, "Diagnosing the origin and impact of low-mode asymmetries in ignition experiments at the National Ignition Facility," Physical Review E **108**, L053203 (2023).
[6]A. L. Kritcher, R. Town, D. Bradley, D. Clark, B. Spears, O. Jones, S. Haan, P. T. Springer, J. Lindl, R. H. H. Scott, D. Callahan, M. J. Edwards, and O. L. Landen, "Metrics for long wavelength asymmetries in inertial confinement fusion implosions on the National Ignition Facility," Physics of Plasmas **21**, 042708 (2014), https://pubs.aip.org/aip/pop/article-pdf/doi/10.1063/1.4871718/15771413/042708_1_online.pdf.
[7]J. D. Kilkenny, P. M. Bell, D. K. Bradley, D. L. Bleuel, J. A. Caggiano, E. L. Dewald, W. W. Hsing, D. H. Kalantar, R. L. Kauffman, D. J. Larson, J. D. Moody, D. H. Schneider, M. B. Schneider, D. A. Shaughnessy, R. T. Shelton, W. Stoeffl, K. Widmann, C. B. Yeamans, S. H. Batha, G. P. Grim, H. W. Herrmann, F. E. Merrill, R. J. Leeper, J. A. Oertel, T. C. Sangster, D. H. Edgell, M. Hohenberger, V. Y. Glebov, S. P. Regan, J. A. Frenje, M. Gatu-Johnson, R. D. Petrasso, H. G. Rinderknecht, A. B. Zylstra, G. W. Cooper, and C. Ruizf, "The National Ignition Facility diagnostic set at the completion of the National Ignition Campaign, september 2012," Fusion Science and Technology **69**, 420–451 (2016), https://doi.org/10.13182/FST15-173.
[8]F. E. Merrill, D. Bower, R. Buckles, D. D. Clark, C. R. Danly, O. B. Drury, J. M. Dzenitis, V. E. Fatherley, D. N. Fittinghoff, R. Gallegos, G. P. Grim, N. Guler, E. N. Loomis, S. Lutz, R. M. Malone, D. D. Martinson, D. Mares, D. J. Morley, G. L. Morgan, J. A. Oertel, I. L. Tregillis, P. L. Volegov, P. B. Weiss, C. H. Wilde, and D. C. Wilson, "The neutron imaging diagnostic at NIF (invited)a)," Review of Scientific Instruments **83**, 10D317 (2012), https://pubs.aip.org/aip/rsi/article-pdf/doi/10.1063/1.4739242/8824963/10d317_1_online.pdf.
[9]A. S. Moore, E. P. Hartouni, D. Schlossberg, S. Kerr, M. Eckart, J. Carrera, L. Ma, C. Waltz, D. Barker, J. Gjemso, E. Mariscal, G. Grim, and J. Kilkenny, "The five line-of-sight neutron time-of-flight (nToF) suite on the National Ignition Facility (NIF)," Review of Scientific Instruments **92**, 023516 (2021), https://pubs.aip.org/aip/rsi/article-pdf/doi/10.1063/5.0040730/15782153/023516_1_online.pdf.
[10]R. M. Bionta, G. P. Grim, K. D. Hahn, E. P. Hartouni, E. A. Henry, H. Y. Khater, A. S. Moore, and D. J. Schlossberg, "Real-time nuclear activation detectors for measuring neutron angular distributions at the National Ignition Facility (invited)," Review of Scientific Instruments **92**, 043527 (2021), https://pubs.aip.org/aip/rsi/article-pdf/doi/10.1063/5.0042869/14031647/043527_1_online.pdf.
[11]P. L. Volegov, S. H. Batha, V. Geppert-Kleinrath, C. R. Danly, F. E. Merrill, C. H. Wilde, D. C. Wilson, D. T. Casey, D. Fittinghoff, B. Appelbe, J. P. Chittenden, A. J. Crilly, and K. McGlinchey, "Density determination of the thermonuclear fuel region in inertial confinement fusion implosions," Journal of Applied Physics **127**, 083301 (2020), https://pubs.aip.org/aip/jap/article-pdf/doi/10.1063/1.5123751/15241041/083301_1_online.pdf.
[12]P. L. Volegov, C. R. Danly, F. E. Merrill, R. Simpson, and C. H. Wilde, "On three-dimensional reconstruction of a neutron/x-ray source from very few two-dimensional projections," Journal of Applied Physics **118**, 205903 (2015), https://pubs.aip.org/aip/jap/article-pdf/doi/10.1063/1.4936319/13983632/205903_1_online.pdf.
[13]K. W. Wong and B. Bachmann, "Three-dimensional electron temperature measurement of inertial confinement fusion hotspots using x-ray emission tomography," Review of Scientific Instruments **93**, 073501 (2022), https://pubs.aip.org/aip/rsi/article-pdf/doi/10.1063/5.0097471/16564506/073501_1_online.pdf.
[14]M. J. Willemink and P. B. No el, "The evolution of image reconstruction for CT—from filtered back projection to artificial intelligence," European Radiology **29**, 2185–2195 (2019).
[15]K. Churnetski, K. M. Woo, W. Theobald, P. B. Radha, R. Betti, V. Gopalaswamy, I. V. Igumenshchev, S. T. Ivancic, M. Michalko, R. C. Shah, C. Stoeckl, C. A. Thomas, and S. P. Regan, "Three-dimensional hot-spot x-ray emission tomography from cryogenic deuterium–tritium direct-drive implosions on OMEGA," Review of Scientific Instruments **93**, 093530 (2022), https://pubs.aip.org/aip/rsi/article-pdf/doi/10.1063/5.0098977/16603737/093530_1_online.pdf.
[16]K. M. Woo, R. Betti, C. A. Thomas, C. Stoeckl, K. Churnetski, C. J. Forrest, Z. L. Mohamed, B. Zirps, S. P. Regan, T. J. B. Collins, W. Theobald, R. C. Shah, O. M. Mannion, D. Patel, D. Cao, J. P. Knauer, V. Y. Glebov, V. N. Goncharov, P. B. Radha, H. G. Rinderknecht, R. Epstein, V. Gopalaswamy, F. J. Marshall, S. T. Ivancic, and E. M. Campbell, "Analysis of core asymmetries in inertial confinement fusion implosions using three-dimensional hot-spot reconstruction," Physics of Plasmas **29**, 082705 (2022), https://pubs.aip.org/aip/pop/article-pdf/doi/10.1063/5.0102167/16603551/082705_1_online.pdf.
[17]J. J. Moré, "The levenberg-marquardt algorithm: Implementation and theory," in *Numerical Analysis*, edited by G. A. Watson (Springer Berlin Heidelberg, Berlin, Heidelberg, 1978) pp. 105–116.
[18]C. B. Choy, D. Xu, and J. Y. Gwak, "3D-R2N2: A unified approach for single and multi-view 3D object reconstruction," (2016), arXiv:1604.00449.
[19]B. T. Wolfe, Z. Han, J. S. Ben-Benjamin, J. L. Kline, D. S. Montgomery, E. C. Merritt, P. A. Keiter, E. Loomis, B. M. Patterson, L. Kuettner, and Z. Wang, "Neural network for 3D inertial confinement fusion shell reconstruction from single radiographs," Review of Scientific Instruments **92**, 033547 (2021), https://pubs.aip.org/aip/rsi/article-pdf/doi/10.1063/5.0043653/13862306/033547_1_online.pdf.
[20]D. T. Casey, High Energy Density Physics (To be submitted).
[21]O. A. Hurricane, D. T. Casey, O. Landen, D. A. Callahan, R. Bionta, S. Haan, A. L. Kritcher, R. Nora, P. K. Patel, P. T. Springer, and A. Zylstra, "Exten-

AIP Publishing
Review of Scientific Instruments
ACCEPTED MANUSCRIPT
This is the author's peer reviewed, accepted manuscript. However, the online version of record will be different from this version once it has been copyedited and typeset.
PLEASE CITE THIS ARTICLE AS DOI: 10.1063/5.0205656

sions of a classical mechanics "piston-model" for understanding the impact of asymmetry on icf implosions: The cases of mode 2, mode 2/1 coupling, time-dependent asymmetry, and the relationship to coast-time," Physics of Plasmas **29**, 012703 (2022), https://pubs.aip.org/aip/pop/article-pdf/doi/10.1063/5.0067699/16626340/012703_1_online.pdf.

[22]D. A. Callahan, O. A. Hurricane, A. L. Kritcher, D. T. Casey, D. E. Hinkel, Y. P. Opachich, H. F. Robey, M. D. Rosen, J. S. Ross, M. S. Rubery, C. V. Young, and A. B. Zylstra, "A simple model to scope out parameter space for indirect drive designs on NIF," Physics of Plasmas **27**, 072704 (2020), https://pubs.aip.org/aip/pop/article-pdf/doi/10.1063/5.0006217/13876362/072704_1_online.pdf.

[23]R. E. Olson, G. A. Rochau, O. L. Landen, and R. J. Leeper, "X-ray ablation rates in inertial confinement fusion capsule materials," Physics of Plasmas **18**, 032706 (2011), https://pubs.aip.org/aip/pop/article-pdf/doi/10.1063/1.3566009/16022617/032706_1_online.pdf.

[24]P. Springer, O. Hurricane, J. Hammer, R. Betti, D. Callahan, E. Campbell, D. Casey, C. Cerjan, D. Cao, E. Dewald, L. Divol, T. Doeppner, M. Edwards, J. Field, C. Forrest, J. Frenje, J. Gaffney, M. Gatu-Johnson, V. Glebov, V. Goncharov, G. Grim, E. Hartouni, R. Hatarik, D. Hinkel, L. B. Hopkins, I. Igumenshchev, P. Knapp, J. Knauer, A. Kritcher, O. Landen, A. Pak, S. L. Pape, T. Ma, A. MacPhee, D. Munro, R. Nora, P. Patel, L. Peterson, P. Radha, S. Regan, H. Rinderknecht, C. Sangster, B. Spears, and C. Stoeckl, "A 3d dynamic model to assess the impacts of low-mode asymmetry, aneurysms and mix-induced radiative loss on capsule performance across inertial confinement fusion platforms," Nuclear Fusion **59**, 032009 (2018).

[25]S. H. Langer, I. Karlin, and M. M. Marinak, "Performance characteristics of HYDRA – a multi-physics simulation code from llnl," in *High Performance Computing for Computational Science – VECPAR 2014*, edited by M. Daydé, O. Marques, and K. Nakajima (Springer International Publishing, Cham, 2015) pp. 173–181.

[26]R. Anirudh, J. J. Thiagarajan, P.-T. Bremer, and B. K. Spears, "Improved surrogates in inertial confinement fusion with manifold and cycle consistencies," Proceedings of the National Academy of Sciences **117**, 9741–9746 (2020), https://www.pnas.org/doi/pdf/10.1073/pnas.1916634117.

[27]B. Kustowski, J. A. Gaffney, B. K. Spears, G. J. Anderson, R. Anirudh, P.-T. Bremer, J. J. Thiagarajan, M. K. G. Kruse, and R. C. Nora, "Suppressing simulation bias in multi-modal data using transfer learning," Machine Learning: Science and Technology **3**, 015035–015052 (2022), https://doi.org/10.1088/2632-2153/ac5e3e.

[28]C. Andrieu, N. de Freitas, A. Doucet, and M. I. Jordan, "An introduction to mcmc for machine learning," Machine Learning **50**, 5–43 (2003).

[29]J. H. Kunimune, H. G. Rinderknecht, P. J. Adrian, P. V. Heuer, S. P. Regan, F. H. Séguin, M. Gatu Johnson, R. P. Bahukutumbi, J. P. Knauer, B. L. Bachmann, and J. A. Frenje, "Knock-on deuteron imaging for diagnosing the morphology of an ICF implosion at OMEGA," Physics of Plasmas **29**, 072711 (2022), https://pubs.aip.org/aip/pop/article-pdf/doi/10.1063/5.0096786/16591450/072711_1_online.pdf.

[30]H. G. Rinderknecht, P. V. Heuer, J. Kunimune, P. J. Adrian, J. P. Knauer, W. Theobald, R. Fairbanks, B. Brannon, L. Ceurvorst, V. Gopalaswamy, C. A. Williams, P. B. Radha, S. P. Regan, M. G. Johnson, F. H. Séguin, and J. A. Frenje, "A knock-on deuteron imager for measurements of fuel and hotspot asymmetry in direct-drive inertial confinement fusion implosions (invited)," Review of Scientific Instruments **93**, 093507 (2022), https://pubs.aip.org/aip/rsi/article-pdf/doi/10.1063/5.0099301/16602110/093507_1_online.pdf.

[31]J. A. Frenje, "Nuclear diagnostics for inertial confinement fusion (ICF) plasmas," Plasma Physics and Controlled Fusion **62** (2020), 10.1088/1361-6587/ab5137.

[32]O. A. Hurricane, D. T. Casey, O. Landen, A. L. Kritcher, R. Nora, P. K. Patel, J. A. Gaffney, K. D. Humbird, J. E. Field, M. K. G. Kruse, J. L. Peterson, and B. K. Spears, "An analytic asymmetric-piston model for the impact of mode-1 shell asymmetry on ICF implosions," Physics of Plasmas **27**, 062704 (2020), https://pubs.aip.org/aip/pop/article-pdf/doi/10.1063/5.0001335/16049679/062704_1_online.pdf.

[33]R. Storn and K. Price, "Differential evolution – a simple and efficient heuristic for global optimization over continuous spaces," Journal of Global Optimization **11**, 341–359 (1997).

[34]B. T. Wolfe, M. J. Falato, X. Zhang, N. T. T. Nguyen-Fotiadis, J. P. Sauppe, P. M. Kozlowski, P. A. Keiter, R. E. Reinovsky, S. A. Batha, and Z. Wang, "Machine learning for detection of 3D features using sparse x-ray tomographic reconstruction," Review of Scientific Instruments **94**, 023504 (2023), https://pubs.aip.org/aip/rsi/article-pdf/doi/10.1063/5.0101681/16682891/023504_1_online.pdf.